

Corona Formation and Heat Loss on Venus by Coupled Upwelling and Delamination

Suzanne E. Smrekar and Ellen R. Stofan

Jet Propulsion Laboratory
California Institute of Technology
MS 183-501
4800 Oak Grove Dr.
Pasadena, CA 911 09

July 9, 1997

Science

Abstract

Coronae are volcanotectonic features that are unique to Venus and are interpreted to be small-scale upwellings. A model in which upwelling causes delamination at the edge of the plume head, along with deformation of a pre-existing depleted mantle layer, can produce the full range of topographic forms of coronae. If half of the coronae are active, delamination of the lower lithosphere could account for about 10% of Venus's heat loss, with another 15% due to upwelling. Delamination may occur in other geologic environments and could help account for Venus' heat loss 'deficit.'

Venus is expected to be as geologically active as Earth because its size, mean density, and radioactive content indicate a comparable heat budget (1). The large and even distribution of unmodified impact craters suggests that Venus was geologically active until about 500 Ma when activity apparently slowed (2). Critical questions for Venus evolution are what caused the decline in activity, how is Venus losing its heat, and why have Venus and Earth evolved so differently.

The tectonic style of a planet is defined by the mechanisms through which the hot, convecting interior, or mantle, transfers heat through the cold, stiff outer layer, called the thermal lithosphere. There are three geologically conventional end member methods of heat loss: (i) hotspot volcanism, (ii), plate recycling (or plate tectonics), and (iii) lithospheric conduction (1). Hotspots, or surface manifestations of large-scale upwelling mantle plumes with broad (1000-2500 km) topographic rises, contribute only a small fraction (<5%) of Venus' heat budget (3). Data from the Magellan mission showed no evidence of global systems of spreading ridges, transform faults, and trenches that characterize terrestrial plate tectonics (4). Models of episodic heat loss (5), proposed to explain the apparent dearth of recent geologic activity, indicate that conduction through the lithosphere may currently be the dominant mechanism, but do not actually predict the geologic signature of global overturn for comparison to observations. The thick lithosphere predicted by these models appears to be inconsistent with even a low level of ongoing volcanism and tectonism. The formation of coronae is consistent with a relatively thin lithosphere and may account for a significant portion of Venus' heat loss through small-scale mantle upwelling and recycling of the lower lithosphere through delamination.

Coronae are nearly circular annuli of fractures and/or ridges (Fig. 1) that are interpreted as manifestations of small-scale mantle upwelling driven by thermal buoyancy (6-8). There are about 360 coronae on Venus, ranging in diameter from ~100 to 2600 km, with most in a diameter range of 200-400 km (7). Below we address many of the outstanding questions in the study of coronae, including why they are unique to Venus, how the full range of topographic profiles are produced, the relationship between topography and the annulus of fractures that characterize coronae, the

subduction zone morphology found on the edges of some coronae (9), and the cause of their complex geologic history (7).

Initial studies of coronae from Magellan radar images defined five classes based primarily on the shape of the annulus: Concentric, asymmetric, multiple, radial/concentric, or concentric-double ring (6). The topographic shapes of the 360 coronae on Venus were classified into nine groups (7) (Table 1). Group 3 includes corona shapes such as an elevated rim surrounding a central dome (Fig. 1), two nested topographic rings, and partial annular rims with irregular interior topography.

Models of corona formation (10-14) predict domes, plateaus, or an elevated interior surrounded by a rim and an outer moat caused by relaxation of a plateau (groups 1, 2, and some of 3, about 25% of coronae). Koch and Manga (15) modeled the formation of a depression with an outer rim (group 4 - 25%), where the depression forms as the rising thermal upwelling spreads out beneath the lithosphere. However, these models predict only domes (10, 11, 13, 14), simplify the thermal and viscosity structure such that surface deformation may be overestimated (15), or require topographic relaxation of an initial steep plateau (10, 12). The shapes not predicted by previous models and the lack of evidence for a plateau stage at many coronae necessitate other explanations for corona formation.

The annuli of coronae are also more complex than previously thought. First observations of coronae indicated that the annulus was composed of concentric compressional ridges (16, 17); later studies using Magellan data indicated that ridges are present, but extensional graben are more common (6, 8). Recent mapping studies indicate that some coronae may go through multiple stages of annulus formation (17). At several coronae, the topographic rim and the tectonic annulus do not coincide. At Idem Kuva Corona (Fig. 1), which belongs to group 3a, the older annulus segment lies outside the deformed, upraised rim (17). This annulus location, and multiple phases of annulus formation, are not predicted by prior models (10-15).

Coronae are not uniformly distributed on Venus (6, 18). Coronae on Venus occur at hotspots (21%), along major rift zones (chasmata) or minor fracture belts (68%), and as relatively isolated features in the plains (11%) (7). Chasmata coronae generally formed coincident with extensional

deformation (7, 19). The deep troughs around some coronae associated with chasmata have been interpreted as evidence for subduction (9, 20). Schubert and Sandwell (9) proposed that chasmata originate at the thinned lithosphere near hotspots; propagation of the rift into the cooler, thicker plains lithosphere results in foundering and subduction. They explain the circularity of coronae to be a coincidence of oppositely subducting arc segments, and suggest that chasmata coronae have a fundamentally different origin than other coronae. However, coronae occur all along chasmata, including quite near and on hotspots, portions of the annular moats of chasmata coronae are not located along the chasmata, most coronae along chasmata are not surrounded by deep troughs, and all coronae are nearly circular. Some coronae in the plains and at hotspots also are surrounded by deep annular moats. This, combined with continuity of fractures across alleged subduction zones (21), suggests that an alternative explanation for trough formation should be sought.

If coronae formed by different mechanisms, one might expect there to be some distinct correlations between annulus shape, topography, and geologic setting (22). The only correlation between annulus shape and topography is that depressions with or without rims (groups 4 and 8) are almost exclusively concentric features. However, all other topographic groups also contain concentric coronae. In addition, no strong correlation exists between the annulus shape classes and geologic setting. The exception is the radial/concentric class, found only along chasmata (6, 7). The only topography-geologic setting correlation is between groups 7 (rim only) and 9 (little or no topography) and the plains setting. In other settings, a wide range of groups can be seen.

We carried out numerical experiments to investigate the effects of plume and lithospheric properties on corona formation (23). The model predicts the time evolution of topography above a plume of finite duration that rises through the mantle, interacts with the lithosphere, and dies out when heat is no longer supplied from below (24). An axisymmetric finite difference scheme describes temperature and chemistry variations along with a penalty function finite element formulation for solving the buoyant viscous flow equations (25). The viscosity is Newtonian, using an Arrhenius form based on a dry olivine flow law (26), and is scaled to 10^{21} Pa s at a mantle temperature of 1300°C. As the emphasis is on modeling the interaction of the plume with

the lithosphere, the computationally-allowed temperature-dependent viscosity variation 0.1×10^4 is focused in that region rather than distributed over the entire area. In some models, a low density layer of mantle residuum is included beneath the lithosphere, and is assumed to be a result of prior melting events. A value of 20% depletion of Fe relative to Mg is used, consistent with the formation of a basaltic crust.

For the one case described in detail (Fig. 2 and 3) the initially 75 km thick lithosphere thickens to ~195 km over the 400 my. duration of the calculation and the mantle temperature decreases by ~20°C because heat is not continuously added to the system. A depleted mantle layer extends from the surface down to 150 km. The hot region at the base of the computational domain feeds the plume for 140 m.y. The plume reaches the lithosphere at ~100 my.; the plume tail rises for ~165 my.

A dome forms as the plume uplifts the lithosphere (132 m.y.) (Figs. 2, 3). As the plume head spreads out and thins the lithosphere, the dome broadens and subsides as the plume is shut off and begins to cool (196 my.). The lithosphere thickens at the edge of the plume head as the plume spreads outward and downward (225 my.). Sinking of the lower lithosphere, or delamination, pulls the surface downward. Delamination is driven initially by flow of the plume head and is sustained by the density difference between the lithosphere and mantle. Viscous flow pulls the delaminating lithosphere towards the center (246 my.), shifting the surface trough. Eventually the trough merges into a central depression (278 m.y.). The depleted mantle layer is pulled downward with the thermal lithosphere. The lowest topographic point is reached when the cold lithosphere pulling downward balances the low density depleted layer pushing upward (304 my.). As the depleted layer continues to thicken, the topography starts to increase (324 my.). Continued thickening of the depleted layer causes a broad topographic ring to form at the center (392 my.).

Other model runs with variations in the plume and lithospheric properties (23) predict somewhat different topographic forms (Table 2). Congestion of the delaminating ring as it moves inward can apply a torque on the ring causing a rim to form outside of the trough (groups 3-6, ~40% of coronae). For a very thick depleted mantle layer, the initial effect when a plume

encounters the layer is to cause a depression at the surface (group 8). For a depression to occur, the positive density anomaly due to thinning of the low density residuum layer relative to the surrounding mantle must be greater than the negative density due to the hot plume. A dome can eventually form at the center of the depression if the plume persists (group 1). If delamination develops and the temperature difference in the lithosphere dissipates before the delaminating lithosphere reaches the center of the corona, isostatic rebound of the depleted mantle creates a ring of high topography (group 7).

These models predict all of the corona groups (Table 2). Groups 3-6 can be produced as a result of early stage delamination, and groups 7-9 can be produced as late stage phases of delamination. Deformation of a depleted mantle layer can produce the interior depressions seen in topographic groups 3b, 4, 5, 6, and 8. Only isostatic rebound of a depleted mantle layer pulled down by delamination produces topographic group 7. This process could also be responsible for some of the rims and rises seen in groups 3-6. Groups 5 and 6 (6% of coronae), have only been produced at larger scales (2000 km diameter). It is possible that these forms require a larger plume diameter/lithospheric thickness ratio than for the cases shown. The implication may be that these forms require a thinner lithosphere.

In addition to predicting the observed topography, the model predictions are consistent with studies of corona geologic history and their general geologic setting. The predicted evolution of the topography is complex, consistent with the observation that coronae topographic highs and fracture annuli do not always coincide. The model predicts that the topography continues to evolve long after the plume thermal anomaly has dissipated, in agreement with observations suggesting a long evolution (17, 27). In addition, the topography and position of the fracture annulus at many coronae varies azimuthally. This irregularity is not predicted by this model, but it is easy to imagine that delamination of the lower lithosphere will not proceed uniformly towards the center for geometric reasons. The model also provides an explanation for topographic troughs as a direct consequence of upwelling and is consistent with estimates of limited convergence (28). However, the viscous model does not predict the observed steep relief of some of the troughs and may

require a weakness in the lithosphere that allows it to break and be more readily pulled downward, such as a rift (9).

We interpret the model predictions and geologic observations as evidence of a depleted mantle layer. The isostatic rebound of a depleted mantle layer pulled downward by delamination is the only model that predicts group 7. This formation mechanism is consistent with the observation that rim formation is a late stage event (17). Additional evidence in favor of the presence of a depleted mantle layer is the predominance of rim only coronae (group 7) and coronae with little topographic relief (group 9) in plains regions. A thicker depleted mantle layer is expected beneath the relatively stable plains regions, just as on Earth a chemical lithosphere is believed to occur beneath continents (29). Further, the correlation between topographic depressions and concentric coronae, and the observation that many of these coronae have no radial fractures, suggests that central uplift may not occur at all coronae. The correlation between a chasmata setting and the radial/concentric class may indicate a lack of depleted mantle at rifts zones, where a thin depleted layer is expected.

Model results indicate that inferring specific plume or lithospheric properties or even the evolutionary stage of a corona is not straightforward. In general, the more complex the deformation and topography, the later the stage of evolution. Geologic history can aid in inferring evolutionary stage. Geologic analyses indicate that annulus shape, topography and geologic setting of coronae are not well correlated. We interpret this lack of correlation as evidence that corona evolutionary stage is usually more important than lithospheric thickness in determining corona morphology.

The contribution to planetary cooling from coronae can be approximated by calculating the buoyancy flux due to the temperature difference between the delaminating ring or plume and the surrounding mantle. Buoyancy flux is defined as Mv , where, M is mass per unit area and v is velocity. The mass is given by $\rho\alpha\Delta T$, where ρ is the reference mantle density (3300 kg/m^3), α is the coefficient of thermal expansion ($3 \times 10^{-5} \text{ K}^{-1}$), and ΔT is the temperature. The buoyancy flux

for the plume (Fig. 2a) at a depth of 600 km below the surface is 2.1 Mg/s. The buoyancy flux of the delaminating lithosphere at a depth of 400 km (Fig. 2d) is 3.0 Mg/s. The 800 km diameter of the model corona (Figs. 2 and 3) is larger than the average corona diameter of about 300 km (6). Since the cross sectional area is proportional to the square of the radius, the average corona buoyancy flux should be a factor of $300^2/800^2$ smaller, or 0.30 Mg/s for the plume and 0.42 Mg/s for the delaminating lithosphere.

The overall contribution by coronae to planetary heat loss is difficult to estimate, as their current level of activity is uncertain. Analysis of crater densities suggest that corona range in age from 0 to ~350 m.y. (30), and mapping studies suggest that many coronae are sites of persistent geologic activity over time (17, 27). To estimate the number of active coronae, we assume that those coronae that have a raised interior (~180 of the 360 coronae) are active since a thermal anomaly is likely to be present under most domes. This may be a conservative estimate, since our model does not require dome-shaped topography at active features. Of these coronae, about half have an outer rim, which could be a result of delamination. If both plumes and delamination are active, this gives a buoyancy flux estimate of 90 coronae \times 0.72 Mg/s = 65 Mg/s. If another 90 coronae have active plumes but are not delaminating, the additional flux would be 90 \times ~0.30 Mg/s = 27 Mg/s.

A precise estimate of buoyancy flux for plumes is difficult due to uncertainties in plume, lithospheric, and mantle properties even for terrestrial hotspots (31) where better constraints are available than for Venus. However, we believe the estimate we present is a reasonable, if not lower, bound due to the long plume duration assumed. The longer the duration of the plumes, the lower the buoyancy flux required to create a given topographic height. We have estimated the buoyancy flux using a plume lasting 140 m.y, in which the corona topography continues to evolve for at least 275 m.y. Considerably longer evolution times are probably unlikely, given the resurfacing age of the planet of ~500 m.y. (2) and indications that coronae are relatively young features (30). Using a model of a cooling thermal diapir, Musser and Squyres (14) find lifetimes of 10s to 100s of m.y.

The estimated buoyancy flux for terrestrial hotspots is $\sim 50 \text{ Mg/s}$, which accounts for about 10% of the total planetary heat loss of $\sim 82 \text{ wMm}^2$ (32). Heat loss for Venus is a matter of debate, but typical estimates range from $35\text{-}65 \text{ wMm}^2$ (33). Based on the higher end of this range, which is appropriate for our models that assume an Earth-like lithospheric thickness, coronae could account for as much as $\sim 25\%$ of the heat flux on Venus.

Delamination in other geologic environments, such as highland plateaus, could also play a role. Competing theories for their origin are upwelling and downwelling. (34, 35). For prior downwelling models, the time scale of deformation was prohibitively long (35). The mechanism of coupled upwelling and delamination proposed here for corona formation may be able to explain more of the characteristics of highland plateau formation than prior models. The final plateau in this model would be a result of isostatic rebound of residuum material pulled downward by delamination. The general geologic history implied by plateau formation through coupled upwelling and delamination appears consistent with the observed structures at some highland plateaus (36). This concept must be demonstrated numerically, but serves to illustrate one possible example of coupled upwelling and delamination in addition to coronae, indicating the potential significance of this process for heat loss on Venus.

The success of the model in explaining why coronae are unique to Venus and in predicting topographic forms, as well as a long, complex deformation history, where other models have failed provides an indication that delamination of the lower lithosphere and deformation of a depleted mantle layer are likely to be occurring on Venus. The overall picture of Venus suggested by these results is one in which a significant amount of heat is lost by delamination of the lower lithosphere and small-scale upwellings. In the absence of large-scale, linear upwellings at ridges and downwellings at subduction zones that characterize terrestrial plate tectonics, small-scale upwellings and delamination may accomplish the same heat loss but result in less disruption of the surface and lower resurfacing rates. On Earth, surface deformation is predominantly a result of large scale lateral translation of plates, which involves deformation of the entire lithosphere. The surface deformation due to vertical motions at hotspots and possible delamination sites is far more

subtle and does not result in resurfacing of the entire region uplifted. For example, at hotspot swells on Earth, resurfacing by volcanism and extension affects only a small fraction of the entire area uplifted. The large resurfacing age on Venus has been interpreted to indicate a thick thermal lithosphere (5, 37). Here we suggest it is simply a result of a different tectonic style. Our results indicate that a thin (~100 km thick) lithosphere may be consistent with both low resurfacing rates and high heat flow. In addition, these results suggest that coronae with typical diameters of several hundred kilometers are inconsistent with lithospheric thicknesses significantly greater than 100 km, consistent with other corona models (12, 38).

The issue of whether or not a change in the style or rate of geologic processes on Venus is required by the crater distribution remains open. Recent work suggests that resurfacing of much of the planet may not have occurred catastrophically but rather over a period of 500 m.y. (39). If widespread lithospheric overturn did occur on Venus, as suggested to explain the resurfacing history (5), such an event could have aided the loss of water from the mantle and the associated mantle-lithospheric decoupling. The loss of a low-viscosity zone might have caused a transition from a more Earth-like style of plate tectonics in which the entire lithosphere is free to deform to one in which a strongly coupled lithosphere and mantle effectively confine the most vigorous deformation to the lower lithosphere (40).

The importance of strong coupling between the lithosphere and mantle (in the absence of a water-related low viscosity zone beneath the lithosphere) in these results furthers the argument that water may be the primary factor shaping the differing tectonic styles of Venus and Earth (41) and presents an explanation for why coronae are unique to Venus. The mechanism of coupled upwelling and downwelling may also be relevant to the problem of the driving force for initiation of subduction (42). There is evidence supporting both a hotter lithosphere and a dehydrated upper mantle in the Archean (43), the earliest period of Earth's geologic history, which suggests strong coupling of the mantle and lower lithosphere may have occurred.

REFERENCES AND NOTES

1. S. C. Solomon and J. W. Head, *J. Geophys. Res.* **87**, 9236 (1982).
2. R. J. Phillips et al., *J. Geophys. Res.* **97**, 15,923 (1992).
3. S. E. Smrekar and E. M. Parmentier, *J. Geophys. Res.* **101**, 5397 (1996).
4. S. C. Solomon et al., *Science* **252**, 297 (1991).
5. E. M. Parmentier and P. C. Hess, *Geophys. Res. Lett.* **19**, 2015 (1992); D. L. Turcotte, *J. Geophys. Res.* **98**, 17,061 (1993).
6. E. R. Stofan et al., *J. Geophys. Res.* **97**, 13,347 (1992).
7. E. R. Stofan, V. E. Hamilton, D. M. Janes, S. E. Smrekar, in *Venus II*, S. W. Brougher, D. M. Hunten, and R. J. Phillips, Eds. (Univ. of Arizona Press, Tucson, 1997) pp. 931-965.
8. S. W. Squyres et al., *J. Geophys. Res.* **97**, 13,611 (1992).
9. G. Schubert and D. T. Sandwell, *Icarus* **117**, 173 (1995).
10. E. R. Stofan, D. L. Bindschadler, J. W. Head, E. M. Parmentier, *J. Geophys. Res.* **96**, 20,933 (1991).
11. D. M. Janes et al., *J. Geophys. Res.* **92**, 16,055 (1992).
12. D. M. Janes and S. W. Squyres, *J. Geophys. Res.* **100**, 21,173 (1995).
13. D. M. Koch, *J. Geophys. Res.* **99**, 2035 (1994).
14. G. S. Musser, Jr. and S. W. Squyres, *J. Geophys. Res.* **102**, 6581 (1997).
15. D. M. Koch and M. Manga, *Geophys. Res. Lett.* **23**, 225 (1996).
16. V. L. Barsukov et al., *J. Geophys. Res.* **91**, 378 (1986); A. A. Pronin and E. R. Stofan, *Icarus* **87**, 452 (1990).
17. D. L. Copp, J. E. Guest, E. R. Stofan, submitted to *J. Geophys. Res.*, (1997).
18. S. W. Squyres et al., *Geophys. Res. Lett.* **20**, 2965 (1993).
19. V. E. Hamilton and E. R. Stofan, *Icarus* **121**, 171 (1996).
20. D. T. Sandwell and G. Schubert, *Science* **257**, 766 (1992).
21. V. L. Hansen and R. J. Phillips, *Science* **260**, 526 (1993).
22. One hypothesis might be that isolated plains coronae form through delamination (peeling away of the lower lithosphere due to density instabilities) and coronae along chasmata are upwellings. Conversely, if coronae all form by the same mechanism, differences in the morphologic characteristics of coronae between each geologic setting may provide constraints on regional lithospheric structure. For instance, the lithosphere along rifts or at hotspots might be thinner than in the plains.
23. A series of 12 numerical cases were run in which plume and lithospheric parameters were varied. Delamination of the lower lithosphere developed in half of these cases. The initial temperature and width of the hot region at the base of the computational domain was varied from 1750°C to 2200°C and 50 to 100 km, respectively. The plume duration varies from 50-430 m.y. The base of the high viscosity thermal lithosphere is defined as the 1100°C contour. The lithospheric thickness range was 50-150 km; the range of residuum layer thickness was 0-200 km, where the thickness is counted as starting at the surface. The radial and vertical dimensions of the computational domain were varied from 250-800 km. In addition to these 12 cases, over 50 cases were run with a radius of 2400 km. These cases were aimed at modeling large-scale hotspot-like features; 15 of these were reported on in Smrekar and Parmentier (1996). As noted in Table 1, a few of the corona topographic groups have only been predicted to date in the larger scale numerical models.
24. The upwelling arises from a 'hot patch' that consists of a high temperature region at the base of the central axis of the computational domain in which temperature decreases linearly away from the axis. There is no attempt to match the depth of the box to a physical boundary such as the core mantle boundary. Rather the computational resources are devoted to modeling the top of the convecting boundary layer (i.e. the lithosphere). Indeed, the origin of upwellings that create coronae is unknown, but is believed to lie in the upper mantle on the basis of coronae size.
There are no rigorous constraints on the duration of plumes on Venus. The maximum duration of plumes on Earth is also poorly constrained due to destruction of the lithosphere, but the oldest probable plume is 200 m.y. (R. White and D. P. McKenzie, *J. Geophys. Res.* **94**,

- 7685, (1989)). Thus the range of plume duration was chosen to be comparable to that of terrestrial plumes while allowing for a large variation. In trying to model plumes that fit the observed range of topography, plume temperature (and thus buoyancy) trades off with plume duration. Again, the temperature of terrestrial plume heads when they reach the base of the lithosphere was used as a guide, with a typical peak temperature when the plume encounters the lithosphere of $\sim 1390^{\circ}\text{C}$ or higher.
25. The finite element grid is 90 by 90 elements; the finite difference grid has twice as many elements. The element spacing is non-uniform to give maximum resolution in the axial upwelling region and in the region where the plume interacts with the lithosphere. The vertical normal stress and shear stress are assumed to vanish on the bottom boundary and on the vertical outer boundary of the cylindrical domain. Boundary conditions are rigid (vanishing horizontal and vertical velocity) at the top of the cylindrical region. The surface and interior temperatures are 500°C and 1300°C , respectively. Non-diffusing chemical variations are calculated using a particle-in-cell type method (K. Jha, E. M. Parmentier, J. Phipps Morgan, *Earth Planet. Sci. Lett.* **125**, 221 (1994)). More details of the numerical approach are given in Smrekar and Parmentier (1996) and references therein.
 26. S. I. Karato, M. S. Paterson, and J. D. Fitzgerald, *J. Geophys. Res.* **96**, 20,947 (1991).
 27. E. R. Stofan and J. E. Guest, *Lunar and Planet. Sci.* **XXVII**, 1277 (1996).
 28. C. D. Brown and R. E. Grimm, *Icarus* **117**, 219 (1995).
 29. T. J. Jordan, *J. Petrol. Special Lithosphere Issue*, 11 (1988).
 30. M. Price and J. Suppe, *Nature* **372**, 756 (1994).
 31. S. Stein and C. A. Stein, *Science* **275**, 1613 (1997).
 32. G. F. Davies, *Earth Planet. Sci. Lett.* **123**, 277 (1992).
 33. R. J. Phillips et al, in *Venus II*, S. W. Brougher, D. M. Hunten, and R. J. Phillips, Eds. (Univ. of Arizona Press, Tucson, 1997).
 34. D. L. Bindschadler and E. M. Parmentier, *J. Geophys. Res.* **95**, 21,329 (1990); R. J. Phillips, R. E. Grimm, and M. C. Malin, *Science* **252**, 651 (1991).
 35. J. G. Kidder and R. J. Phillips, *J. Geophys. Res. Planet.* **101**, 23,181 (1996); A. Lenardic, D. M. Koch, W. M. Kaula, D. L. Bindschadler, *J. Geophys. Res. Plan.* **100**, 16,949 (1995).
 36. V. L. Hansen and R. J. Phillips, *Geology* **23**, 292 (1995).
 37. S. C. Solomon, *Phys. Today* **46**, 48 (1993); W. B. Moore and G. Schubert, *Geophys. Res. Lett.* **22**, 429 (1995); V. S. Solomatov and L.-N. Moresi, *J. Geophys. Res.* **101**, 5397 (1996).
 38. K. E. Cyr and H. J. Melosh, *Icarus* **102**, 175 (1993).
 39. S. A. Hauck II, R. J. Phillips, and M. Price, *Lunar Planet. Sci. Conf. XXVIII*, 527 (1997).
 40. R. J. Phillips, W. M. Kaula, G. E. McGill, M. C. Malin, *Science* **212**, 879 (1981).
 41. W. M. Kaula, *Geophys. Res. Lett.* **17**, 1401 (1990); W. M. Kaula, *Science* **270**, 1490 (1995); R. J. Phillips, *J. Geophys. Res.* **95**, 1301 (1990).
 42. S. Mueller and R. J. Phillips, *J. Geophys. Res.* **96**, 651 (1991).
 43. P. H. Warren, *Geology* **12**, 335 (1984).
 44. This work was supported by National Aeronautics and Space Administration (NASA) Planetary Geology and Geophysics Program grant 15 I-01-70-71 to SES and 151-01-70-59" to ERS. The JPL/Caltech Cray Supercomputer used in this investigation was provided by funding from the NASA (Offices of Mission to Planet Earth, Aeronautics, and Space Science. We thank Marc Parmentier for the use of his numerical code and Jeffery Fall and Eric DeJong for their assistance in creating the Magellan topography and image overlay. The research presented in this paper was carried out at the Jet Propulsion Laboratory, California Institute of Technology, under a contract with **NASA**.

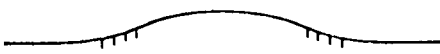
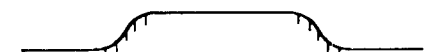
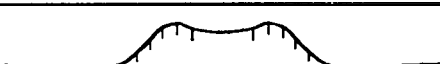






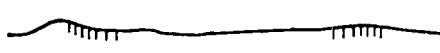
Group	Topographic Profile	Description	% of Coronae
1		Dome	10
2		Plateau	10
3a		Rim surrounding interior high	21 (a+b)
3b		Rim surrounding interior dome	
4		Rim surrounding depression	25
5		Outer rise, trough, rim, inner high	5
6		Outer rise, trough, rim, inner low	1
7		Rim only	7
8		Depression	7
9		No discernible signature	14

Table 1. Topographic Groups. Vertical tick marks on topographic profiles indicate the typical location of annuli for each group.

Topographic Elements	Formation Mechanisms
Interior Forms:	
Dome	1) Uplift by hot plume 2) Isostatic uplift of a depleted mantle layer thickened by delamination
Depression	1) Late stage isostatic adjustment of thinned lithosphere 2) Early stage thinning of depleted mantle layer 3) Suction above delaminating ring migrating towards interior
Plateau	1) Relaxation of dome above cooling plume
No Relief	1) Thinning of depleted layer 2) Final stage of thermal equilibration after plume cools
Exterior Forms:	
Outer Rim	1) Isostatic rebound of depleted material after delaminating ring equilibrates 2) Viscous relaxation of plateau 3) Congestion of delaminating ring
Trough	1) Suction above delaminating ring

Table 2. Corona topographic element formation mechanisms.

Figure Captions

Fig. 1. Perspective image of Idem Kuva corona, diameter 280 km. This corona has a raised rim and an inner dome like structure, and is the source of several long lava flows. The main portion of the fracture annulus lies along an elevated outer rim. A portion of an older, flooded annulus can be seen in the foreground (middle right), outside the current topographic rim. This image was produced by combining the Magellan radar image and altimetric data; the vertical exaggeration is 10x. The false color is based on images of the surface returned by Venera landers.

Fig. 2. This figure shows the time evolution of the temperature, compositional and flow fields. Arrows indicate the direction and relative magnitude of the viscous flow. Temperature is shown with color, with blue cold and red hot. White contours are at 1325°C, 1350°C, and 1500°C. Depletion at 1, 5, and 10% is shown with black contours. The 1% contour is the lowermost line.

Fig. 3. Topography for the same time steps as illustrated in Figure 2. Arrows trace the sequence of time steps. Note that the topography is reflected about the vertical axis to show the entire profile across the upwelling, contrary to Figure 2 where the computational domain is shown without reflection.



Figure 1

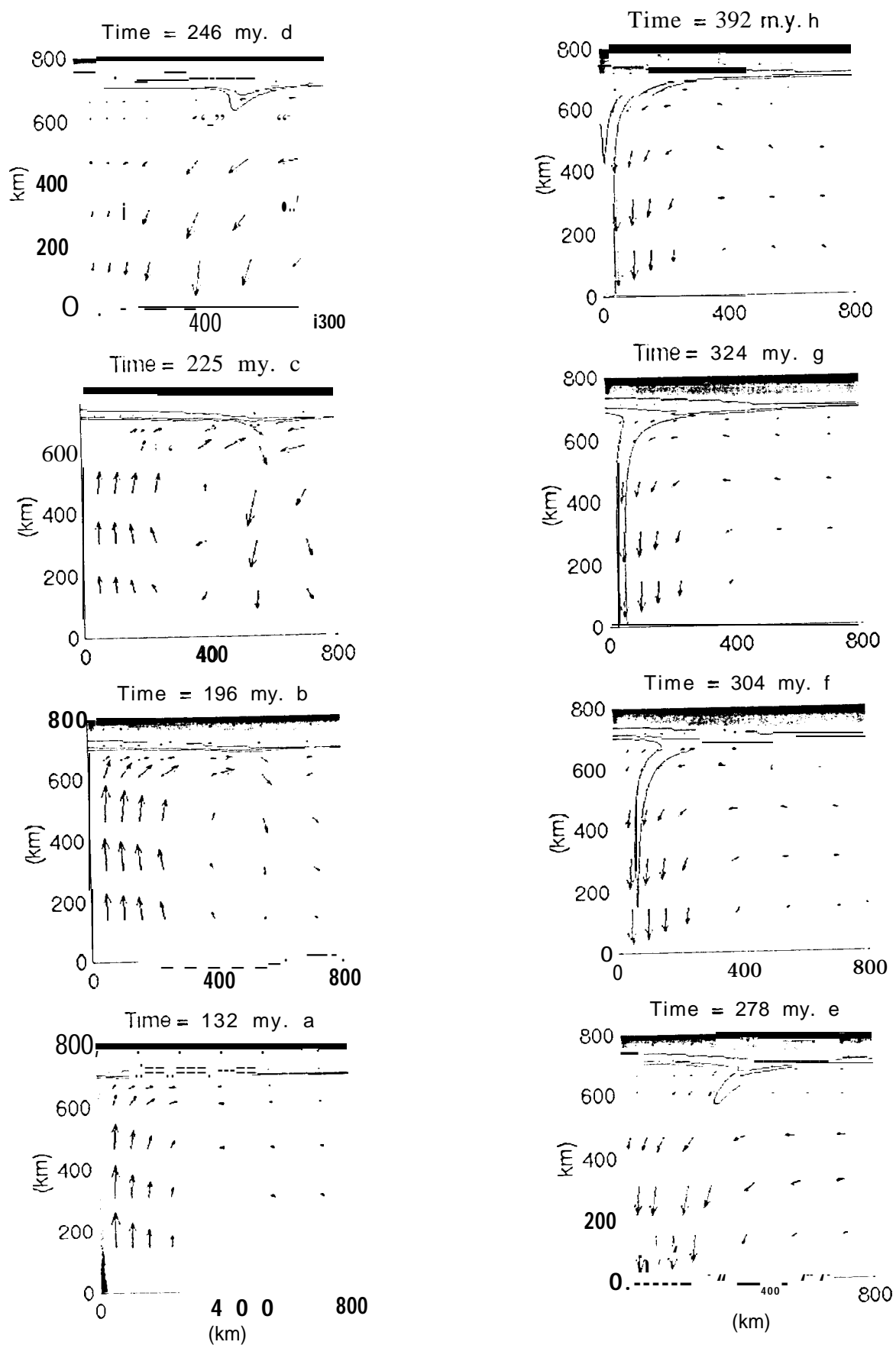


Figure 2

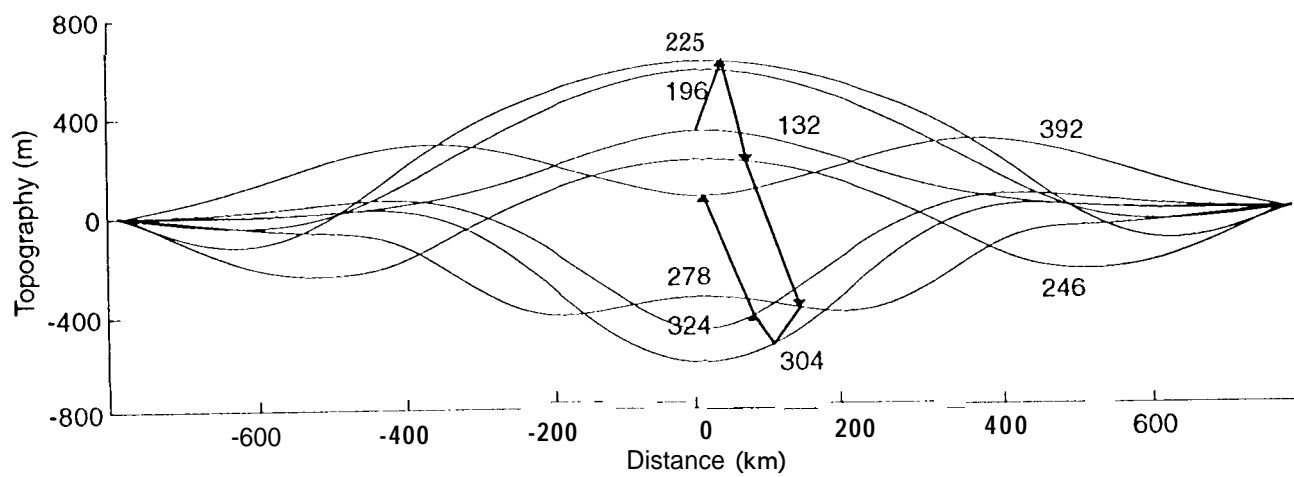


Figure 3